Chapter 3

Dynamics of Multicellular Synthetic Gene Networks

Ekkehard Ullner[1], Aneta Koseska[2], Alexey Zaikin[3,4], Evgenii Volkov[5], Jürgen Kurths[2,6,7], Jordi García-Ojalvo[1]

[1]*Departament de Física i Enginyeria Nuclear, Universitat Politècnica de Catalunya, Colom 11, E–08222 Terrassa, Spain*
[2]*Center for Dynamics of Complex Systems, University of Potsdam, D–14469 Potsdam, Germany*
[3]*Department of Mathematics, University of Essex, Wivenhoe Park, Colchester C04 3SQ, UK*
[4]*Departments of Mathematics & Institute of Women Health, University College London, Gower Street, London WC1E 6BT, UK*
[5]*Department of Theoretical Physics, Lebedev Physical Inst., Leninskii 53, Moscow, Russia*
[6]*Institute of Physics, Humboldt University Berlin, D-10099 Berlin, Germany*
[7]*Potsdam Institute for Climate Impact Research, D-14412 Potsdam, Germany*

3.1. Introduction

Living systems are driven by intricate networks of genes and proteins, whose dynamical behavior underlies all kinds of structural and functional processes in cells. Understanding the dynamics that emerges from such complex networks has benefited greatly in recent years by synthetic approaches, through which simpler network modules have been built that perform natural-like dynamical processes without interfering with, nor being perturbed by, natural cellular processes [for a review, see e.g. Sprinzak and Elowitz (2005)].

One of the first examples of an artificial gene circuit was the *repressilator*, a synthetic biological oscillator developed in *E. coli* from a network of three transcriptional repressors that inhibit one another in a cyclic way [Elowitz and Leibler (2000)]. Spontaneous oscillations were initially observed in individual cells within a growing culture, although substantial variability and noise was present among the different cells. After its conception, the repressilator immediately has become a milestone example of how natural dynamical processes can be mimicked within cells through the design of artificial circuits built from standard genetic parts. Other examples of such genetic gene circuits included a toggle switch [Gardner *et al.* (2000)],

a metabolic relaxator [Fung *et al.* (2005)], or a relaxation oscillator [Atkinson *et al.* (2003)].

Natural genetic networks, however, do not usually operate in isolation. Not only in multicellular higher organisms, but even in bacterial populations, cells conspicuously communicate among each other by different means, e.g. electrically or chemically. A particularly useful (and common) means of communication between bacteria is *quorum sensing*, which relies of the relatively free diffusion of small molecules, known as autoinducers, through the bacterial membrane. When such an autoinducer is part of a feedback loop that regulates the expression of certain genes, bacteria are able to determine the local density of similar cells around them by monitoring the level of expression of these autoinducer-controlled genes [Miller and Bassler (2001)]. An example of this mechanism is provided by the Lux system, used by the bacterium *Vibrio fischeri* to provide bioluminiscence only when the bacterial density is high (which happens within specialized light organs of certain marine organisms with whom the bacteria live in symbiosis).

Cell-cell coupling often leads to exceptional examples of cooperative behavior. In order to understand how such collective phenomena emerge from passive intercellular communication, it seems natural to make use of the synthetic approaches described above. The Lux system described above has been used, for instance, as a communication module to build a synthetic mechanism for programmed population control in a bacterial population [You *et al.* (2004)]. In this Chapter, we review recent developments that are helping us to understand the rich dynamical behavior that can be produced in coupled synthetic gene networks. We concentrate on two different types of genetic oscillators, the repressilator and a relaxator oscillator, and consider two different types of coupling, namely a phase-attractive and a phase-repulsive coupling, both resulting from the autoinducer diffusion. As we will see, many different dynamical scenarios arise from these types of coupling, including multistability, oscillation death, and quantized cycling, among others.

3.2. Coupled Repressilators

As mentioned above, the repressilator is a synthetic network of three genes whose products inhibit the transcription of each other cyclically [Elowitz and Leibler (2000)] (see left module of Fig. 3.1). A readout module using fluorescent proteins provides access to the time-resolved dynamics of the repressilator proteins. Experiments reveal oscillations with a period of the order of an hour, i.e. slower than the cell-division cycle. The limited number of interacting genes and proteins and the well-understood interactions between them enable a precise theoretical description of this oscillator by means of coupled differential equations.

3.2.1. *Phase-attractive coupling*

Quorum sensing has been theoretically shown to lead to synchronization in ensembles of identical genetic oscillators [McMillen *et al.* (2002)]. The oscillators

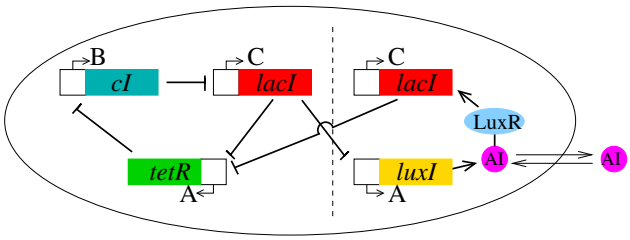

Fig. 3.1. Scheme of the repressilator network coupled to a quorum-sensing mechanism. The original repressilator module is located at the left of the vertical dashed line, while the coupling module appears at the right.

considered in that work were relaxational, analogous to neural oscillators. The repressilator, on the other hand, is sinusoidal rather than relaxational. Furthermore, in the experimental implementation of the repressilator [Elowitz and Leibler (2000)], individual cells were found to oscillate in a "noisy" fashion, exhibiting cell-cell variation in period length, as well as variation from period to period within a single cell.

Accordingly, it seems natural to consider the effect of inter-cell signaling on a population of non-identical and noisy repressilators coupled by reinforcing quorum sensing. Using computational modeling, García-Ojalvo *et al.* (2004) showed that a diverse population of such oscillators is able to self-synchronize, even if the periods of the individual cells are broadly distributed. The onset of synchronization is sudden, not gradual, as a function of varying cell density. In other words, the system exhibits a phase transition to mutual synchrony. This behavior has been experimentally reported in the zebrafish somitogenesis clock [Riedel-Kruse *et al.* (2007)].

The coupling also has a second beneficial effect: it reduces the system's noisiness, effectively transforming an ensemble of "sloppy" clocks into a very reliable collective oscillator [Enright (1980); Somers and Kopell (1995); Needleman *et al.* (2001)]. The results of García-Ojalvo *et al.* (2004) suggest that the constraints that local cell oscillators have to face in order to be noise resistant, could be relaxed in the presence of intercell coupling, since coupling itself provides a powerful mechanism of noise resistance.

3.2.1.1. *Model*

The repressilator consists of three genes, *lacI*, *tetR*, and *cI*, whose protein products repress transcription of the genes cyclically [Elowitz and Leibler (2000)]. García-Ojalvo *et al.* (2004) proposed to incorporate the quorum-sensing system of the bacterium *Vibrio fischeri* as an inter-cell signaling module, by placing the gene that encodes LuxI under the control of the repressilator protein LacI, as shown in Fig. 3.1. LuxI synthesizes a small molecule, the autoinducer (AI), that diffuses freely among the cells and thus couples them to one another. A second copy of another of the

repressilator's genes (such as *lacI*) is inserted into the genetic machinery of the *E. coli* cell in such a way that its expression is induced by the complex LuxR-AI. The result is the appearance of a feedback loop in the repressilator, which is reinforced the more similar among neighboring cells the levels of LacI are.

The mRNA dynamics is governed by degradation and repressible transcription for the repressilator genes, plus transcriptional activation of the additional copy of the *lacI* gene:

$$\frac{da_i}{dt} = -a_i + \frac{\alpha}{1 + C_i^n} \tag{3.1}$$

$$\frac{db_i}{dt} = -b_i + \frac{\alpha}{1 + A_i^n}\,, \tag{3.2}$$

$$\frac{dc_i}{dt} = -c_i + \frac{\alpha}{1 + B_i^n} + \frac{\kappa S_i}{1 + S_i}\,. \tag{3.3}$$

Here a_i, b_i, and c_i are the concentrations in cell i of mRNA transcribed from *tetR*, *cI*, and *lacI*, respectively, and the concentration of the corresponding proteins are represented by A_i, B_i, and C_i (note that the two *lacI* transcripts are assumed to be identical). The concentration of AI inside each cell is denoted by S_i. A certain amount of cooperativity is assumed in the repression mechanisms via the Hill coefficient n, whereas the AI activation is chosen to follow a standard Michaelis-Menten kinetics. The protein and AI concentrations are scaled by their Michaelis constants. α is the dimensionless transcription rate in the absence of a repressor, and κ is the maximal contribution to *lacI* transcription in the presence of saturating amounts of AI. The protein dynamics is given by:

$$\frac{dA_i}{dt} = \beta_a(a_i - A_i)\,, \tag{3.4}$$

and similarly for B_i (with b_i) and C_i (with c_i). The parameter β_a is the ratio between the mRNA and protein lifetimes of A (resp. β_b and β_c, all three are considered equal in this Section). The mRNA concentrations have been rescaled by their translation efficiency (proteins produced per mRNA, assumed equal for the three genes).

Finally, the dynamical evolution of the intracellular AI concentration is affected by degradation, synthesis and diffusion toward/from the intercellular medium. The dynamics of TetR and LuxI can be assumed identical if their lifetimes are considered to be the same, and hence we will use the same variable to describe both variables. Consequently, the synthesis term of the AI rate equation will be proportional to A_i:

$$\frac{dS_i}{dt} = -k_{s0}S_i + k_{s1}A_i - \eta(S_i - S_e)\,, \tag{3.5}$$

where $\eta = \sigma\mathcal{A}/V_c \equiv \delta/V_c$ measures the diffusion rate of AI across the cell membrane, with σ representing the membrane permeability, $\mathcal{A}$ its surface area, and V_c the cell volume. The parameters k_{s0}, k_{s1}, and η have been made dimensionless by time

rescaling. S_e represents the extracellular concentration of AI, whose dynamics is given by

$$\frac{dS_e}{dt} = -k_{se}S_e + \eta_{\text{ext}} \sum_{j=1}^{N} (S_j - S_e) \equiv -k_{se}S_e + k_{\text{diff}}(\overline{S} - S_e), \tag{3.6}$$

where $\eta_{\text{ext}} = \delta/V_{\text{ext}}$, with V_{ext} being the total extracellular volume, and $\overline{\cdots}$ indicates average over all cells. The diffusion rate is given by $k_{\text{diff}} = \eta_{\text{ext}}N$ and the degradation rate by k_{se}. This approach assumes a uniform AI concentration throughout the cell culture, which describes reasonably well the situation encountered in a well-controlled chemostat.

In the quasi-steady-state approximation [McMillen *et al.* (2002); Dockery and Keener (2001)], the extracellular AI concentration can be approximated by

$$S_e = \frac{k_{\text{diff}}}{k_{se} + k_{\text{diff}}} \overline{S} \equiv Q\,\overline{S}\,. \tag{3.7}$$

From the definition of k_{diff} given above, we note that Q depends on the cell density $N/(V_{\text{ext}} + V_c) \approx N/V_{\text{ext}}$ according to

$$Q = \frac{\delta N/V_{\text{ext}}}{k_{se} + \delta N/V_{\text{ext}}}\,. \tag{3.8}$$

In other words, Q is linearly proportional to the cell density provided $\delta N/V_{\text{ext}}$ is sufficiently smaller than the extracellular AI degradation rate k_{se}. In the following the effect of reinforcing quorum-sensing coupling on the collective behavior of model (3.1)-(3.5) is analyzed, with S_e defined by (3.7)-(3.8), considering Q (and hence the cell density) as a control parameter.

3.2.1.2. *Transition to synchronization*

In the hypothetical case of infinite cell dilution ($Q \to 0$), the system consists of a population of uncoupled limit-cycle oscillators. Each individual cell clock is an extension of the original repressilator [Elowitz and Leibler (2000)], where a new degree of freedom has been added to the original six-dimensional phase space to represent the intracellular AI dynamics (3.5). The resulting dynamical system exhibits limit-cycle oscillations in a wide region of parameter space. The characteristic oscillations of the repressilator [Elowitz and Leibler (2000)] do not change qualitatively in the presence of the AI dynamics.

The oscillator population will likely contain substantial differences from cell to cell (e.g. extrinsic noise [Elowitz *et al.* (2002)]), giving rise to a relatively broad distribution in the frequencies of the individual clocks at any given time. The variability in the cell population is modeled by considering that β ($\equiv \beta_a = \beta_b = \beta_c$) is non-uniformly distributed among the repressilators following a Gaussian law with standard deviation $\Delta\beta$. The corresponding frequency distribution of a group of 10^4 uncoupled cells for $\Delta\beta/\beta = 0.05$ is shown in Fig. 3.2(a). The temporal evolution of

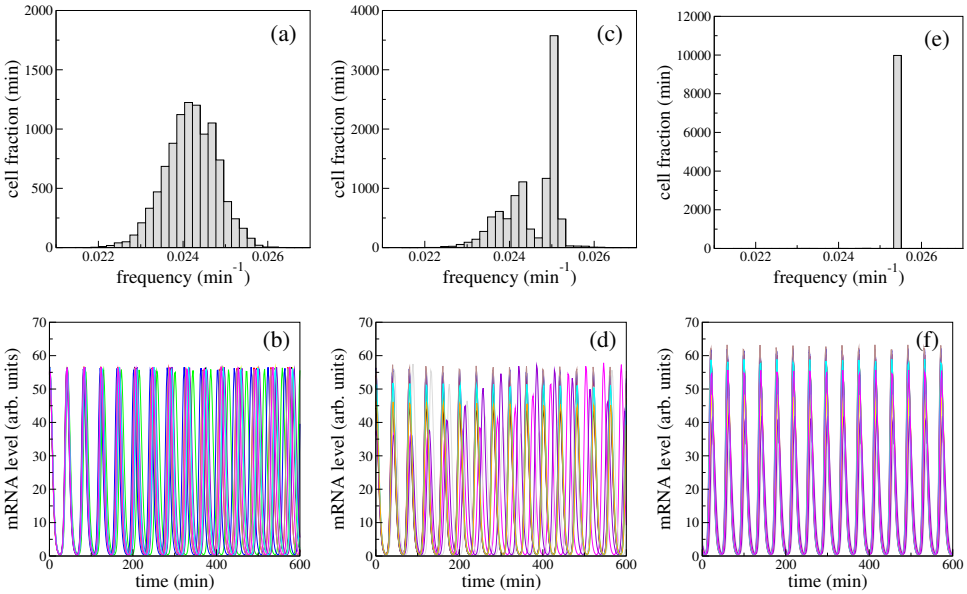

Fig. 3.2. Frequency histogram (a, c, e) and time evolution of $b_i(t)$ for 10 cells (b, d, f) and increasing cell density: (a, b) $Q = 0.4$, (c, d) $Q = 0.63$, (e, f) $Q = 0.8$. Other parameters are $N = 10^4$, $\alpha = 216$, $\kappa = 20$, $n = 2.0$, $k_{s0} = 1$, $\eta = 2.0$ and $k_{s1} = 0.01$. The lifetime ratio β in the different cells is chosen from a random Gaussian distribution of mean $\bar{\beta} = 1.0$ and standard deviation $\Delta\beta = 0.05$.

the *cI* mRNA concentration in 10 of those cells is plotted in Fig. 3.2(b), showing how the global operation of the system is completely disorganized, so that no collective rhythm can exist under these conditions.

As the cell density increases, diffusion of extracellular AI molecules into the cells provides a mechanism of intercell coupling, which leads to partial frequency locking of the cells [Figs. 3.2(c,d)]. Finally, when the cell density is large enough [Figs. 3.2(e,f)] perfect locking and synchronized oscillations are observed. In that case the system behaves as a macroscopic clock with a well-defined period, even though it is composed of a widely varied collection of oscillators. This results indicate that a transition from an unsynchronized to a synchronized regime exists as the strength of coupling increases (due to an increase in cell density). This behavior is robust in the presence of noise. In fact, noise can be seen to enhance the collective coherence of the system, leading to a better clock [García-Ojalvo *et al.* (2004)].

3.2.2. *Phase-repulsive coupling*

We now show how significantly can cell-cell coupling influence the dynamics of synthetic gene network. Only one rewiring in the connectivity between the basic repressilator and the quorum sensing module, with respect to the case of the

previous Section, alters the coupling from its original reinforcing character to a phase-repulsive one [Ullner *et al.* (2007)]. As a consequence, the previously favored in-phase regime becomes now unstable, and many new dynamical regimes appear.

To create a phase-repulsive coupling, one can modify the initial scheme (Fig. 3.1) by placing the gene *luxI* under inhibitory control of the repressilator protein TetR. The proposed 'rewiring' between the repressilator and the quorum sensing module introduces a feedback loop that competes with the overall negative feedback loop along the repressilator ring, resulting in a phase-repulsive intercellular coupling.

The mRNA and protein dynamics are described by Eqs. (3.1)–(3.4) above. In contrast to Section 3.2.1, we assume here different lifetime ratios for the protein/mRNA pairs, which results in a weak relaxator-like dynamics of the repressilator. The rewiring affects the equation of the AI concentration. Now the AI concentration S_i in cell i is generated at a rhythm proportional to B_i:

$$\dot{S}_i = -k_{s0} S_i + k_{s1} B_i - \eta(S_i - S_e)\,. \tag{3.9}$$

A moderate increase of the Hill coefficient to $n = 2.6$, a value in agreement with recent experimental measures [Rosenfeld *et al.* (2005)], together with different lifetime ratios $\beta_a = 0.85$, $\beta_b = 0.1$, and $\beta_c = 0.1$, increase the nonlinear character of the repressilator dynamics, leading to the appearance of two time scales in the time series, with a fast concentration increase and a relative slow decay. The slower protein decay increases the period of the repressilator by a factor of approximately three.

3.2.2.1. *Bifurcation analysis for two coupled repressilators*

A first glimpse into the effect of coupling on the dynamics of inter-cell genetic networks can be obtained by investigating a minimal system of only two oscillators. Figure 3.3 shows representative time traces, obtained by direct numerical calculations of a population of $N = 2$ coupled repressilators for increasing coupling strength. The different dynamical regimes found are self-sustained oscillatory solutions [Fig. 3.3(a)], inhomogeneous limit cycles (IHLC) [Fig. 3.3(b)], inhomogeneous steady states (IHSS) [Fig. 3.3(c)] and homogeneous steady states (HSS) [Fig. 3.3(d)], all of which exist for biologically realistic parameter ranges.

A detailed bifurcation analysis allows to determine the origin of these different solutions and the transition scenarios between them, thus providing deeper qualitative and quantitative conclusions about the structure and dynamical behavior of the system. This analysis can be performed with public software such as the XPPAUT package [Ermentrout (2002)]. In the bifurcation analysis below we use the coupling strength Q [Eq. (3.7)] as a biologically relevant parameter to obtain one-parameter continuation diagrams. Starting from the homogeneous unstable steady state of isolated oscillators ($Q = 0$), Fig. 3.4 shows the basic continuation curve containing the homogeneous and inhomogeneous stable steady states.

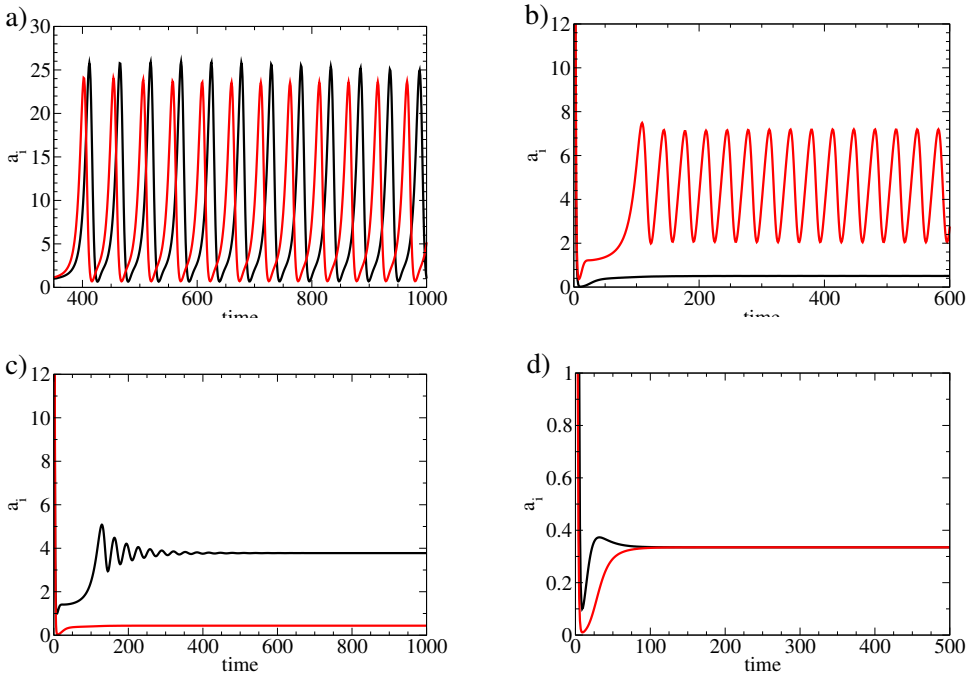

Fig. 3.3. Typical time series of the a_i mRNA concentration for the four stable regimes: a) $Q = 0.1$ – oscillatory, b) $Q = 0.3$ – inhomogeneous limit cycle, c) $Q = 0.4$ – inhomogeneous steady state, and d) $Q = 0.4$ – homogeneous steady state. The common parameters are: $N = 2$, $n = 2.6$, $\alpha = 216$, $\beta_a = 0.85$, $\beta_b = 0.1$, $\beta_c = 0.1$, $\kappa = 25$, $k_{s0} = 1.0$, $k_{s1} = 0.01$, $\eta = 2.0$.

The basic continuation curve is characterized by two important properties: (1) the presence of broken symmetry bifurcations (BP_1 and BP_2 in Fig. 3.4) where inhomogeneous solutions arise, and (2) the stabilization of the homogeneous state for large coupling values ($Q > 0.129$). The HSS solution is characterized by a constant protein level concentration, stabilized through a saddle node bifurcation (LP_1 in Fig. 3.4). A typical time series of this regime can be seen in Fig. 3.3(d). Additionally, another HSS branch is found between LP_4 and HB_4 (Fig. 3.4), but it is located outside the biologically relevant range (since $Q > 1$).

As a result of the symmetry breaking of the system through a pitchfork bifurcation (BP_1 in Fig. 3.4), the unstable steady state splits in two additional branches, giving rise to an inhomogeneous steady state (IHSS). This particular phenomenon is model-independent, persisting for large parametric regions in several models of diffusively coupled chemical [Bar-Eli (1985); Dolnik and Marek (1988); Crowley and Epstein (1989)] or biological oscillators [Kuznetsov *et al.* (2004); Tsaneva-Atanasova *et al.* (2006)]. The IHSS in the present model is manifested through two distinct steady protein concentration levels [Fig. 3.3(c)], gaining stability through a Hopf bifurcation, denoted as HB_1 in Fig. 3.4, and thus leading to the so-called "oscillation death" (OD) regime. This regime arises at a critical coupling $Q_{crit} = 0.3588$ for

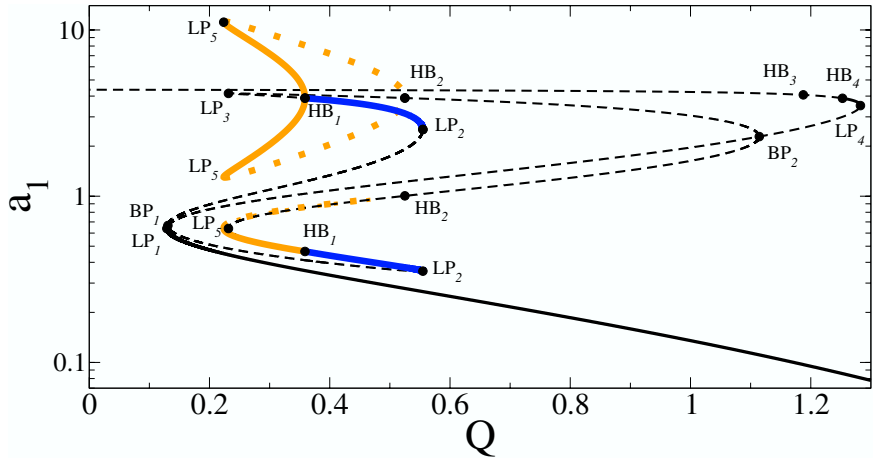

Fig. 3.4. Bifurcation diagram obtained by variation of Q, illustrating the stable steady state regimes (HSS and IHSS) and the inhomogenous limit cycle (IHLC). For parameters values see Fig. 3.3. Here, thin solid lines denote the HSS, thick blue solid lines the IHSS, thick solid orange line the stable IHLC, and dashed lines denote the unstable steady states especially the dashed orange line the unstable IHLC. The same bifurcation diagram is valid for the second repressilator.

the set of parameters used here, and is stable until LP_2 at $Q = 0.5548$. The IHSS solution coexists in the Q parameter space with the HSS (Fig. 3.4). For example, for $Q = 0.37$ there is a coexistence of 9 steady state solutions, 3 of them stable and 6 unstable.

The next step of the bifurcation analysis is to study the limit cycles that arise from the Hopf bifurcations found on the basic continuation curve. In particular, the Hopf bifurcation HB_1 gives rise to a branch of stable inhomogeneous periodic solutions, known in the literature as inhomogeneous limit cycle (IHLC) [Tyson and Kauffman (1975)]. The manifestation of this regime is however different in different systems: for two identical diffusively coupled Brusselators, e.g., it is defined to be a periodic solution of the system of oscillators rotating around two spatially non uniform centers [Tyson and Kauffman (1975); Volkov and Romanov (1995)]. For the model investigated here, the manifestation of the IHLC is somewhat different: the IHLC is characterized by a complex behavior, where one of the oscillators produces very small oscillations of the protein level, whereas the other one oscillates in the vicinity of the steady state with an amplitude 4 times smaller than that of an isolated oscillator [see Fig. 3.3(b)]. The IHLC is stable for values of Q between HB_1 and LP_5 (Fig. 3.4). In the case of the two-oscillator system considered here, each oscillator has the same probability to occupy and stay in the upper or lower state, due to the symmetry of the system. The initial conditions are the only factor determining the separation of the oscillators.

For coupling values smaller than a given critical value $Q_{crit} < 0.129$, the system is characterized by a self-oscillatory solution. For two coupled oscillators, this regime

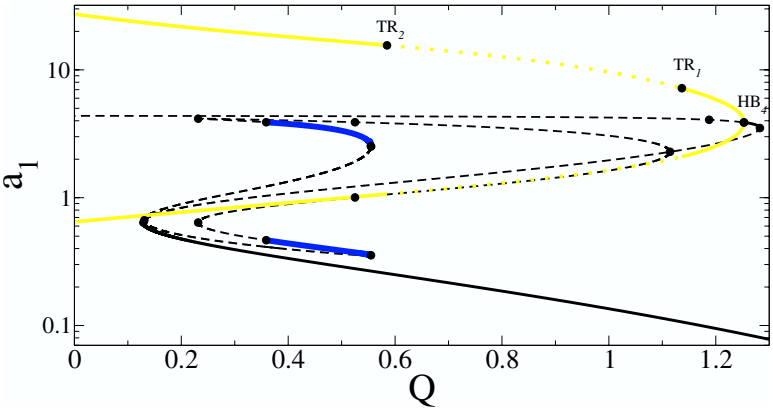

Fig. 3.5. Bifurcation diagram versus coupling Q, focusing on the stable anti-phase oscillations (thick yellow line). Parameters are those of Fig. 3.3.

corresponds to anti-phase oscillations. As shown on Fig. 3.5, this state belongs to a branch of periodic orbits originating at the Hopf bifurcation HB_4. Fig. 3.5 illustrates in detail the bifurcation structure of the antiphase dynamics when Q is being varied. Stable anti-phase oscillations are observed between HB_4 ($Q = 1.253$) and TR_1 (torus bifurcation for $Q = 1.137$), and from $Q = 0$ until TR_2 ($Q = 0.5848$). As demonstrated, this solution loses its stability for $0.5848 < Q < 1.137$. Direct numerical simulations revealed the existence of complex behavior in the latter range of Q values, which we discuss in detail in the next Section.

In contrast to the case of positively coupled repressilators [García-Ojalvo *et al.* (2004)], where coupling was seen to provide coherence enhancement, investigations of the dynamical structure of the system with phase-repulsive coupling by means of direct calculations [Ullner *et al.* (2007)] did not reveal the presence of an stable in-phase regime (synchronous oscillations over the entire cell population). The present bifurcation analysis confirms this result: a branch of synchronous periodic oscillations is in fact seen to emanate from HB_3, but it is unstable (data not shown, see Ullner *et al.* (2008)). The bifurcation analysis confirmed that the in-phase regime is unstable for all values of α and Q studied, in contrast to the anti-phase limit cycle oscillations, which arise even for small α values. The existence of this anti-phase (or phase-shifted) solution is a clear manifestation of the phase repulsive character of the AI-mediated coupling, which enhances the phase difference between the oscillators in the model, until the maximal phase difference of $\frac{\pi}{2}$ is reached.

3.2.2.2. *Comparison between bifurcation analysis and direct calculations*

Bifurcation analyses reveal all solutions, their stability, and the connecting bifurcation points. Special interest evokes the ranges of multi-stability, i.e. the coexistence of dynamical regimes, because it offers opportunities of the biological system to

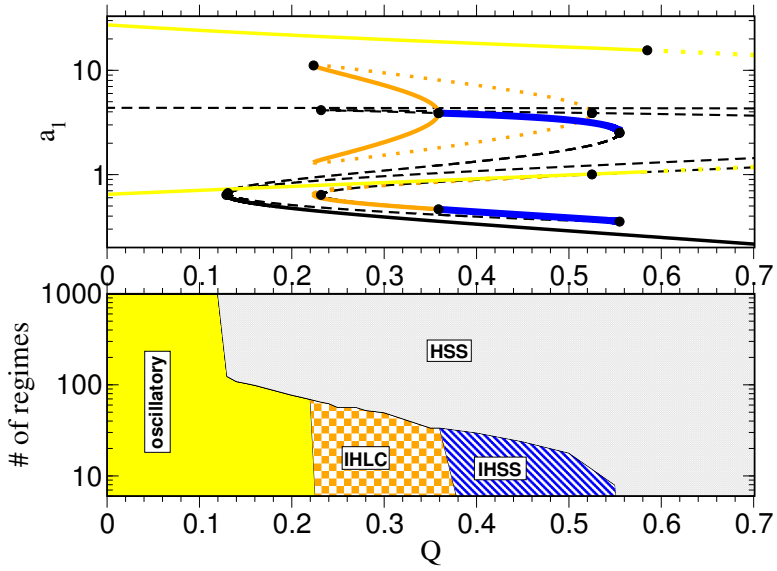

Fig. 3.6. Comparison between the bifurcation analysis (top) and the direct calculation with random initial conditions (bottom). Note the logarithmic scale of both ordinates in the two plots. The oscillatory regime is represented by a yellow solid line (top) and a yellow area (bottom); the IHLC by solid orange lines (top) and a orange-white chess board pattern (bottom); the IHSS by solid blue lines (top) and a small blue striped area (bottom); and finally the HSS is illustrated by a solid black line (top) and a grey area (bottom). Parameters are those of Fig. 3.3.

adapt or to store information. On the other hand, only stable regimes with a sufficient basin of attractions play a role in biological systems, an information that is not in the scope of the bifurcation analysis. The basins of attraction can be quantified in direct numerical simulations from the probability of occurrence of the different dynamical regimes for a set of randomly and appropriately drawn initial conditions. In what follows, we show results for 1000 time series with random initial conditions. Figure 3.6 shows a histogram of the resulting regimes as the bifurcation parameter Q is varied (bottom), compared with the bifurcation plot resulting from the continuation analysis described in the previous Section. Both methods indicate that for small coupling, $Q < 0.129$, anti-phase self-oscillations are the only stable regime. At $Q = 0.129$ the homogenous steady state stabilizes through a limit point bifurcation (LP_1 in Fig. 3.4), coexisting with an oscillatory solution. The direct calculations reveal the dominance of the single-fixed-point solution, which has a larger basin of attraction: at $Q = 0.2$, for instance, only about 70 of the total 1000 random initial conditions result in the oscillatory state, while the other remaining 930 result in HSS. For $Q \in [0.2236, 0.3588]$, direct calculations show the existence of an inhomogenous limit cycle (orange white chessboard pattern in Fig. 3.6,bottom) that coincides with the region where a stable IHLC solution was found by the bifurcation analysis (solid orange line in Fig. 3.6,top). One can see a very good coincidence of

the stability ranges of the IHLC and the IHSS predicted by the bifurcation analysis and shown by the direct calculation. Both regimes have a small basin of attraction.

3.2.2.3. *Chaos provoked by repressive cell-to-cell communication*

The bifurcation analysis (Fig. 3.5) predicts unstable anti-phase oscillations between the torus bifurcation points TR_2 and TR_1. To find the stable solutions emerging from those bifurcations, one can perform direct simulations starting with small coupling Q, and trace the self-oscillatory regime up to strong coupling. The resulting self-oscillations are stable and resistant to small perturbations in the initial conditions and to dynamical noise. Interestingly, these stable self-oscillations display very different dynamics with erratic amplitude and period, which is associated with a positive maximal Lyapunov exponent, and thus corresponds to chaotic dynamics. For a detailed description of the chaotic features of this regime and its validation see Ullner *et al.* (2008).

3.2.2.4. *Large system sizes*

Typically, bacterial colonies consist of many cells and hence the results of the minimal system with $N = 2$ repressilators have to be validated in large ensembles. Here we show results for an ensemble of $N = 100$ coupled identical cells obtained from direct calculations with random initial conditions. Figure 3.7 plots the resulting frequency of stable regimes for increasing Q. The four main regimes HSS, IHSS, IHLC and self-oscillations already observed in the minimal system can be detected in the large systems too.

The results shown in Fig. 3.7 reveal a transition from self-oscillations to a single stable fixed point as the coupling Q increases. This transition is gradual, and

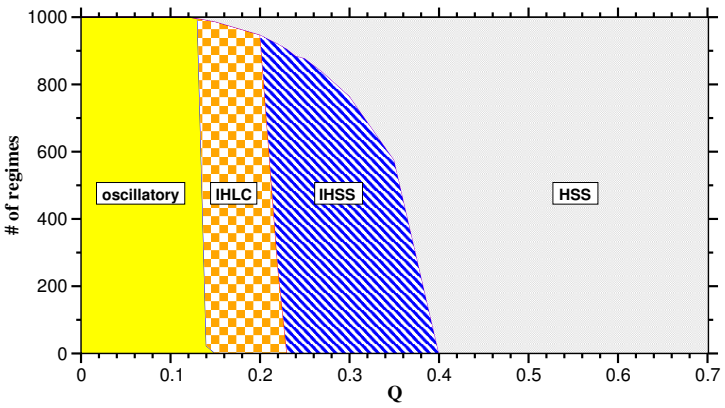

Fig. 3.7. Distribution of stable regimes for increasing coupling strength Q. The parameters are: $N = 100$, $n = 2.6$, $\alpha = 216$, $\beta_a = 0.85$, $\beta_b = 0.1$, $\beta_c = 0.1$, $\kappa = 25$, $k_{s0} = 1.0$, $k_{s1} = 0.01$, and $\eta = 2.0$.

exhibits a multiplicity of regimes. For $Q \lesssim 0.13$ only self-oscillations are found. As in the case $N = 2$, this regime is characterized by large oscillations with the same amplitude and period for all repressilators. The repressive character of the coupling destabilizes the in-phase dynamics, and leads to a spreading of the phases among all oscillators. After a certain transient time, oscillatory clusters appear [Golomb *et al.* (1992); Kaneko and Yomo (1994); Wang *et al.* (2000)]. The population self-organizes into three clusters of cells that oscillate with a phase difference close to $2\pi/3$. The separation into three clusters could provide the population of cells with high reliability and stress resistance, because at any given time the cells in the different clusters are in different states of the limit cycle, and hence each cluster will be affected differently by sudden environmental stresses such as chemicals or lack of nutrients.

At $Q \approx 0.13$ the basin of the self-oscillatory regime disappears abruptly, and a new dynamical regime arises in which some of the cells become trapped in a quasi-steady state with a negligible amplitude, while the rest undergo small amplitude oscillations in protein concentration. This dynamical regime corresponds to an inhomogeneous limit cycle (IHLC), in which cells do not switch from one regime to the other, i.e. there is no mixing of the two populations. As in the minimal case of $N = 2$, the basin of the IHLC coexists with the basin of the HSS, as shown in Fig. 3.7. This single fixed point attractor becomes more likely for larger coupling strengths Q.

At $Q \approx 0.2$, a second abrupt transition takes place, through which the IHLC disappears and the IHSS regime, corresponding to the fully developed oscillation death, arises. In this regime all cells stop oscillating, but they do so differentiating into two different clusters. Since each cluster is specialized in the production of a different protein, this regime could be interpreted as a mechanism of artificial differentiation in an isogenic population of cells. As in the case of the IHLC, cells may distribute into the two clusters at high and low CI levels in many different ratios which differ slightly in the constant protein levels. Hence in fact many different attractors exist, and a fine tuning of protein production can be achieved. Again, the basin of the IHSS regime described coexists with the basin of the single fixed point attractor, which becomes increasingly more likely for increasing Q, until it turns into the dominant attractor of the system for $Q \gtrsim 0.4$.

The dynamical regimes described above and their multistability persist even in a noisy environment. For instance, protein fluctuations larger than 25% of their mean level do not alter the clustering attractor in the multistable parameter range. Interestingly, a comparison of Figs. 3.6 and 3.7 show that the IHLC and the IHSS regimes become much more likely in large systems, at the expense of the HSS. Furthermore, those two regimes appear for smaller coupling in large systems. Together, these results show that the IHLC and the IHSS regimes become more likely in a large ensemble of identical cells than in a small one.

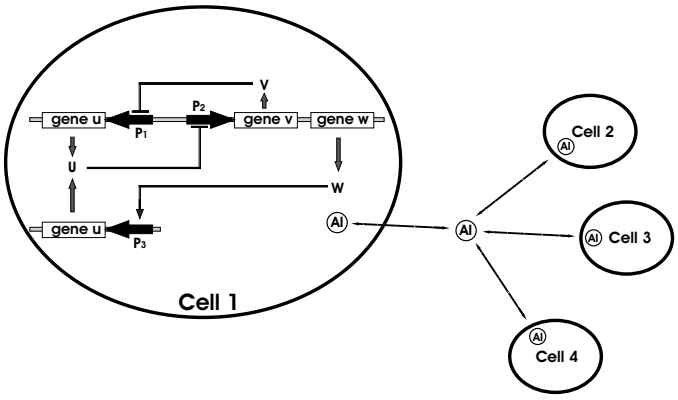

Fig. 3.8. Schematic diagram of the network of genetic relaxation oscillators. u, v and w denote the genes, and P_1, P_2 and P_3 the corresponding promoters.

3.3. Genetic Relaxation Oscillators

Different types of genetic circuit architectures, besides the repressilator, can give rise to oscillations and dynamical behavior. We now consider a different kind of network, consisting of coupled hysteresis-based genetic relaxation oscillators [Kuznetsov *et al.* (2004)]. Studying this system allows the identification of the intercellular mechanisms responsible for multirhythmicity in coupled genetic circuits. Additionally, this system exhibits a dynamical behavior closely related to a known biological problem, namely the existence of quantized cycles in cellular processes.

3.3.1. *Dynamical regimes of coupled relaxators*

Recently, Kuznetsov *et al.* (2004) proposed a model of hysteresis-based relaxation genetic oscillators coupled via quorum-sensing. This oscillator can be constructed, as shown in Fig. 3.8, by combining two engineered gene networks, the toggle switch [Gardner *et al.* (2000)] and an intercell communication system, which have been previously implemented experimentally in *E. coli* by Kobayashi *et al.* (2004), and in *V. fischeri* by Fuqua and Greenberg (2002), respectively. The synthesis of the two repressor proteins, which constitute the toggle switch, are regulated such that the expression of the two genes is mutually exclusive, which leads to bistability. The second network is based on the dynamics of an AI, which on the one hand drives the toggle switch through the hysteresis loop, and on the other hand provides an intercell communication by diffusion through the cell membrane. The time evolution of the system is governed by the dimensionless equations [Kuznetsov *et al.* (2004)]:

$$\frac{du_i}{dt} = \alpha_1 f(v_i) - u_i + \alpha_3 h(\omega_i) \tag{3.10}$$

$$\frac{dv_i}{dt} = \alpha_2 g(u_i) - v_i \tag{3.11}$$

$$\frac{d\omega_i}{dt} = \varepsilon(\alpha_4 g(u_i) - \omega_i) + 2d(\omega_e - \omega_i) \tag{3.12}$$

$$\frac{d\omega_e}{dt} = \frac{d_e}{N}\sum_{i=1}^{N}(\omega_i - \omega_e) \tag{3.13}$$

where N is the total number of cells, u_i and v_i represent the proteins from which the toggle switch is constructed in the i-th cell, w_i represents the intracellular, and w_e the extracellular AI concentration. The mutual influence of the genes is defined by the functions:

$$f(v) = \frac{1}{1+v^\beta}\,, \qquad g(u) = \frac{1}{1+u^\gamma}\,, \qquad h(w) = \frac{w^\eta}{1+w^\eta}\,.$$

Here β, η and γ are the parameters of the corresponding activatory or inhibitory Hill functions.

In the Eqs. (3.10)-(3.13), the dimensionless parameters α_1 and α_2 regulate the repressor operation in the toggle switch, α_3 denotes the activation due to the AI, and α_4 the repression of the AI. The coupling coefficients in the system are given by d and d_e (intracellular and extracellular) and depend mainly on the diffusion properties of the membrane, as well as on the ratio between the volume of the cells and the extracellular volume [Kuznetsov *et al.* (2004)]. If the parameter ε is small ($\varepsilon \ll 1$), as in our case, the evolution of the system splits into two well-separated time-scales, a fast dynamics of u_i, v_i and w_e, and a slow dynamics of w_i. Due to the presence of multiple time scales, the system can produce relaxation oscillations.

The particular organization of the intercellular signaling mechanism in this case allows coupling to be organized through the slow recovery variable in the genetic network. As is known from oscillation theory, such coupling has the phase-repulsive property and can be referred to as inhibitory. On the other hand, local coupling of limit cycles via inhibitory variables has been reported to yield a coexistence of different stable attractors [Volkov and Stolyarov (1991, 1994)], thus leading typically to multirhythmicity.

The main manifestation of multistability in systems of globally coupled oscillators is clustering, defined as a dynamical state characterized by the coexistence of several subgroups, where the oscillators exhibit identical behavior. Oscillator clustering has been proved theoretically for identical phase oscillators [Okuda (1993)], observed experimentally for salt-water oscillators [Miyakawa and Yamada (2001)] and electrochemical oscillators [Wang *et al.* (2001); Kiss and Hudson (2003)]. For a detailed recent review of synchronization in oscillatory networks see [Osipov *et al.* (2007)]. As already mentioned in the repressilator case, the effects of multirhythmicity and multistability can be very important in understanding of evolutionary mechanisms behind cell differentiation and genetic clocks.

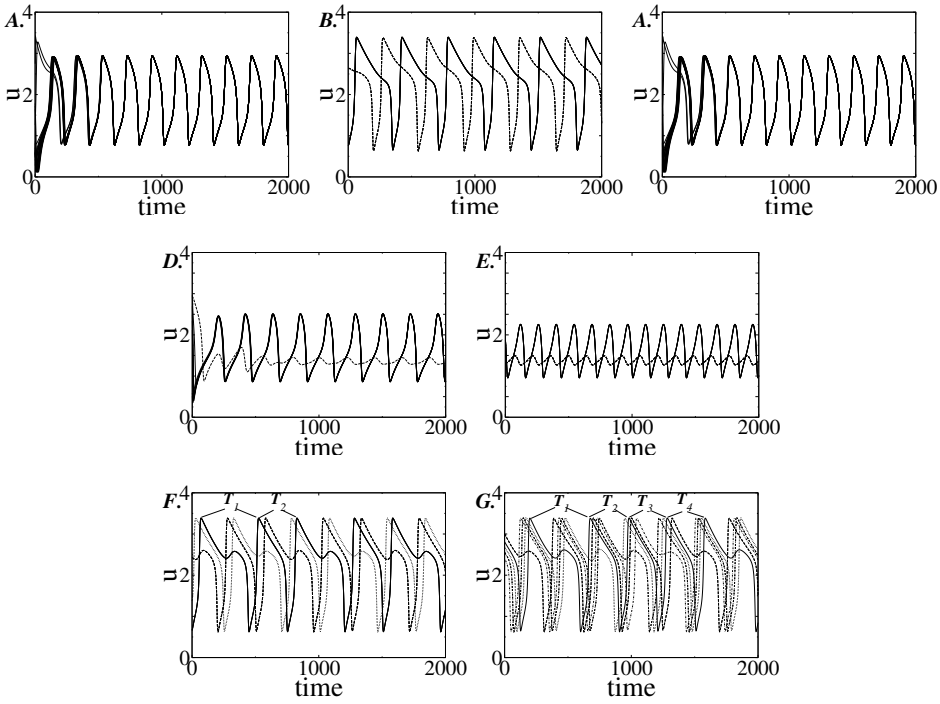

Fig. 3.9. Different oscillatory clusters for a system of $N = 8$ oscillators. A: In-phase oscillations for $\alpha_1 = 3, d = 0.005, d_e = 1$. B, C: Anti-phase oscillations with different distributions of the oscillators between the clusters, for $\alpha_1 = 3.3$, $d = 0.001$. D, E: Asymmetric solution with different distribution of the oscillators, for $\alpha_1 = 2.868$, $d = 0.001$. F: Three oscillatory clusters for $\alpha_1 = 3.3$, $d = 0.00105$. G: Five oscillatory clusters for $\alpha_1 = 3.3$, $d = 0.001$.

We discuss here two main phenomena. First, we show the existence of different possible modes of organized collective behavior in the system of globally coupled relaxation genetic oscillators. We distinguish between two different types of clusters: (i) steady-state clusters, and (ii) oscillatory clusters. Second, for each separate cluster formation, we demonstrate how the dependence on initial conditions can lead to different distributions of the oscillators between the clusters. In general, a system consisting of N oscillators can exhibit $N - 1$ different distributions of the oscillators among the clusters.

When the cells are identical, the coupled system is symmetric and identical behavior of the cells is a solution (Fig. 3.9A), though not necessarily stable. The inhibitory coupling and the presence of multiple time scales, as previously discussed, create the possibility for multistability and multirhythmicity, resulting in the generation of various dynamical regimes, among which oscillatory clusters are formed. For $d < 0.01$, the system can exhibit anti-phase oscillations, with oscillators distributed between the two oscillatory clusters (Fig. 3.9B,C). An important feature to be mentioned is the characterization of different distributions with different periods of the limit cycle, providing more complex dynamics with different rhythms: com-

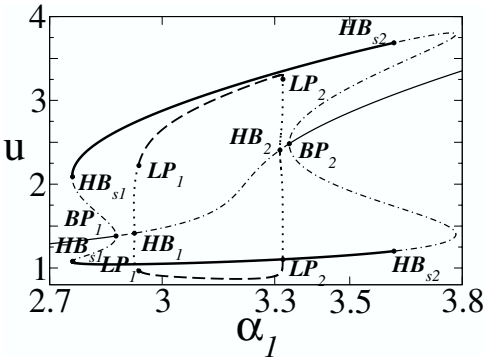

Fig. 3.10. Coexistence of five different states for increased coupling strength $d = 0.3$. Other parameters are: $\alpha_2 = 5$, $\alpha_3 = 1$, $\alpha_4 = 4$, $\beta = \eta = \gamma = 2$, $d_e = 1$ and $\varepsilon = 0.05$. Coexistence of the OD and the in-phase oscillatory regime is also shown.

pare for instance Fig. 3.9B (5:3 distribution) with period $T = 364.15$ and Fig. 3.9C (4:4 distribution) with period $T = 256.27$.

Another possible collective behavior of this system consists in asymmetric oscillations (for $d < 0.003$), when some of the oscillators in the system perform large excursions, while the rest oscillate in the vicinity of a stable steady state with small amplitude. This results in the presence of two oscillatory clusters, (Fig. 3.9D,E). Again, the number of possible different distributions for a system of N oscillators is $N - 1$, and each has different oscillation period: compare Fig. 3.9D (1:7) with period $T = 216.95$ and Fig. 3.9E (4:4) with $T = 141.01$.

The oscillators in the system can be also ordered in multiple cluster regimes; we present only two examples here: three (Fig. 3.9F) and five (Fig. 3.9G) oscillatory clusters. Again, different distributions of the oscillators between the clusters are possible in this case. To illustrate this, we present here a 3:3:2 distribution when three oscillatory clusters are formed (Fig. 3.9F), and a 1:2:2:2:1 distribution when five oscillatory clusters are created (Fig. 3.9G).

3.3.2. *Bifurcation analysis*

Bifurcation analysis can be used to identify and characterize the different dynamical solutions described above. When applied to the case $N = 2$, it shows that already two oscillators provide a large variety of possible regimes, as shown in Fig. 3.10. The OD regime, similarly to the IHSS one, is a result of the symmetry breaking in the system through a pitchfork bifurcation (labeled BP_1 in Fig. 3.10). The unstable steady-state splits into two branches that gain stability through Hopf bifurcations, denoted as HB_{s1} and HB_{s2} in Fig. 3.10. The solution coexists in the α_1-parameter space with different oscillatory solutions, e.g. in-phase oscillations (marked with dashed lines), as shown in Fig. 3.10. The true IHLC that emerges from HB_{s1} is unstable in this model and not shown in Fig. 3.10.

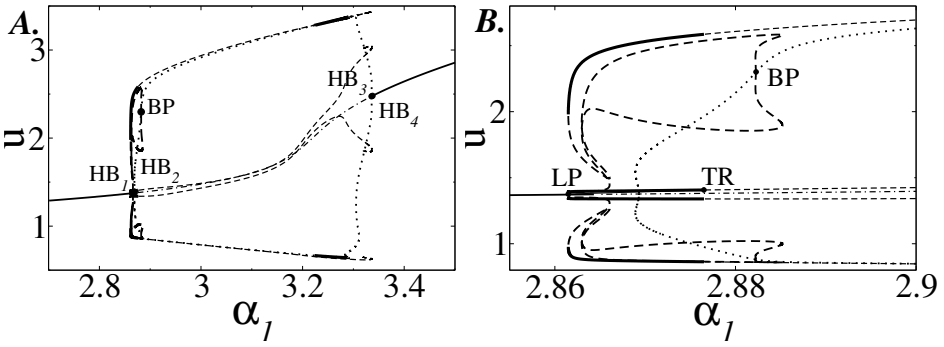

Fig. 3.11. **A**, bifurcation diagram obtained by variation in α_1. Other parameters: $\alpha_2 = 5$, $\alpha_3 = 1$, $\alpha_4 = 4$, $\beta = \eta = \gamma = 2$, $d = 0.001$, $d_e = 1$ and $\epsilon = 0.01$. **B**, detailed view of the region where stable asymmetric solution exists. Between LP and TR, one oscillator has a large amplitude and the other oscillates with small amplitude.

The Hopf bifurcations labeled HB_1 and HB_2 in Fig. 3.10 give rise to a branch of periodic orbits, corresponding to a synchronous in-phase solution (see Fig. 3.9A). The stability of this region is determined with two saddle-node bifurcations LP_1 and LP_2. It is important to note that the in-phase oscillations present in the system are stable for all values of d, in contrast with the case of coupled repressilators discussed above.

For small coupling ($d < 0.01$) anti-phase oscillations arise (Fig. 3.9B,C). The periodic branch giving rise to the anti-phase solution is limited again by two Hopf bifurcations: HB_2 at $\alpha_1 = 2.869$, and HB_3 at $\alpha_1 = 3.336$. However, their stability region is significantly smaller than the corresponding stability region in the repressilator model discussed in Sec. 3.2.2.

Another mode of collective behavior is the asymmetric regime, characterized by the presence of large and small amplitude oscillations (see Fig. 3.9D,E). Although this solution resembles the IHLC shown in 3.2.2, its bifurcation structure here is completely different and very complex. In particular, for $\alpha_1 = 2.882$ a pitchfork bifurcation (labeled BP in Fig. 3.11A,B) is found on the bifurcation branch that gives rise to the anti-phase oscillations. Starting from this bifurcation point, a secondary bifurcation branch with a complex structure is observed (Fig. 3.11A). The stable asymmetric solution lies within this branch; the stability region is depicted with thick lines in Fig. 3.11B (zoomed region where a stable asymmetric solution exists), the unstable asymmetric solution is shown with the dashed line. The asymmetric regime is stabilized through a torus bifurcation at $\alpha_1 = 2.877$ (labeled as TR in Fig. 3.11B). This bifurcation leads to two incommensurate frequencies. For isolated oscillators ($d = 0$) and for $\alpha_1 > \alpha_{HB_1}$, the first frequency is that of a large cycle, and the second one is determined by the eigenvalues of the unstable focus. Slight diversity in the ensemble of relaxators does not alter the behavior shown above (results not shown) and confirms the relevance of these findings for biological networks.

3.3.3. *Response to external noise: quantized cycling time*

The presence of multistability influences the response of the system to external stimuli, in particular noise. This response can be modeled by substituting Eq. (3.13) above by:

$$\frac{d\omega_i}{dt} = \varepsilon(\alpha_4 g(u_i) - \omega_i) + 2d(\omega_e - \omega_i) + \xi_i(t)\,. \tag{3.14}$$

Let us consider the case when all oscillators are confined to the oscillatory region. In order to establish the effect of noise in a population of such genetic units, we quantify the histogram of cycling times, analogous to the inter-spike interval (ISI) histograms used in studies of neural dynamics. We find that noise contributes to the establishment of variability and leads to multiple frequencies [Fig. 3.12(a,b)], even when the oscillators are initially synchronized. The cycling is now quantized, having either a bimodal [Fig. 3.12(a)] or a polymodal [Fig. 3.12(b)] distribution of periods. Thus, choosing slightly different α_1 values, one can effectively switch between different multipeak distributions. The ISI peaks observed are determined by the probability density to find phase points near the jumping threshold between the stochastic version of the attractors revealed by the bifurcation analysis above [Koseska *et al.* (2007a)]. The modes in the polymodal histogram might be separated by almost equal intervals if one of the stochastic attractors dominates over the others, or by different intervals in the opposite case. The same interplay between attractors disrupts the exponential decay of the peak amplitudes that is typical for a noisy attractor under the influence of a periodic signal [Longtin (1995)].

These results indicate that the interplay between intercell signaling and stochasticity might explain the emergence of quantized cycles, a concept that is central in the research of time-dependent biological processes, such as the cell cycle [Lloyd and Volkov (1990)]. Clear experimental evidence for quantized cycles has been obtained

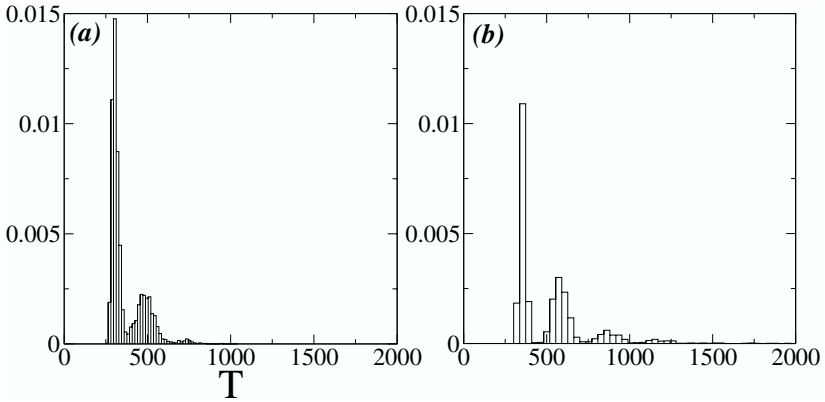

Fig. 3.12. (a) Bimodal ISI distribution for 8 identical oscillators ($\alpha_1 = 3.3$), and (b) polymodal ISI distribution ($\alpha_1 = 3.328$). The noise intensity is $\sigma_a^2 = 5 \cdot 10^{-7}$.

for *Chinese hamster V*79 cells [Klevecz (1976)] and *wee*1$^-$ *cdc25*Δ fission yeast cells [Sveiczer *et al.* (1996)], among others.

The variability in the system behavior can be significantly enhanced when the network becomes slightly inhomogeneous (due for instance to different α_1 values in different cells) in the presence of noise. Another important effect that arises in this system is the possibility to observe maximal variability for an optimal noise intensity. This is in contrast to the well-known effect of coherence resonance [Pikovsky and Kurths (1997)], where for intermediate noise intensities, maximal order can be achieved in systems with underlying nonlinear dynamics [Koseska *et al.* (2007b)]. The results also show that, although organized in a population, different oscillators are characterized by different ISI distributions, as a consequence of the specific, repulsive coupling considered.

3.4. Conclusions and Discussion

The concept of synthetic genetic networks is becoming increasingly exploited as a basic step to understand how cellular processes arise from the connectivity of genes and proteins. The ability of these circuits to produce different rhythms, as has been shown in this Chapter, could have important applications in functional genomics, gene and cell therapy, etc., since the multistability and multirhythmicity of synthetic genetic networks leads to an extended functionality, improved adaptation and ability to store information. On the other hand, one could more easily relate different biological phenomena and extract functional conclusions by observing a highly-adaptive synthetic genetic network, instead of a network producing a unified rhythm.

Here we have reviewed the possibility to use a modular coupling mechanism via quorum sensing, which leads to synchronization under realistic conditions in an ensemble of existing synthetic repressilators. By its design, the communication module can be added directly to existing repressilator strains and mimic natural multicellular clocks that operate on mean periods resulting from averaging multiple cells [Liu *et al.* (1997); Herzog *et al.* (1998); Honma *et al.* (1998); Nakamura *et al.* (2001); Herzog *et al.* (2004)]. Besides its efficiency, the synchronization reported here has been seen to lead to the generation of a global rhythm in a highly heterogeneous ensemble of genetic oscillators. The resulting clock behavior is seen to be highly robust to random phase drifts of the individual oscillators due to noise. In the light of these results, one might speculate whether natural biological clocks have evolved in this same way, i.e. by using inter-cell communication to couple an assembly of originally independent sloppy clocks. The cell-to-cell communication module can also be coupled with the individual genetic circuit in such a way that coupling is phase-repulsive [Ullner *et al.* (2007)].

Beside its biological consequences and extended functionality, the coupling mechanism discussed here leads to new phenomena from a general nonlinear dynamics

viewpoint. First, the oscillation death (OD) described above is stable far from any Hopf bifurcation in a wide range of parameter space. This contrasts with other situations [Herrero *et al.* (2000); Wang *et al.* (2000)], where OD occurred only in a small range close to a Hopf bifurcation. Second, the phase-repulsive character of the coupling leads to multistability between the regimes of OD, IHLC and the single fixed point. The simultaneous availability of these different dynamical regimes to the cellular population improves its adaptability and robustness. Such an improved efficiency induced by coupling can probably exist in natural genetic networks, and can be definitely exploited in synthetic devices. The theoretical predictions reported here are amenable to experimental observation at the single-cell level via time-lapse fluorescence microscopy [Rosenfeld *et al.* (2005)]. This technique is very useful to experimentally test theoretical predictions in genetic networks [Süel *et al.* (2007)].

The results discussed here lead to several open questions in the field of synthetic biology of genetic networks. One of them is the influence of stochasticity arising from the small number of reactant molecules involved in gene regulation (sometimes around 1 mRNA molecule per cell in average), which can lead to significant fluctuations in intracellular mRNA and protein concentrations [Ozbudak *et al.* (2002); Elowitz *et al.* (2002)]. Hence it is important to understand how the variety of dynamical regimes discussed here will change in the presence of noise. Here one should distinguish intrinsic and extrinsic noise acting upon the gene regulation process [Swain *et al.* (2002)]. For the simulations with intrinsic noise usually the Gillespie algorithm is used [Gillespie (1977)], whereas in some situations the chemical Langevin equation approach can be employed [Gillespie (2000)]. In the system presented here, the dynamics can be expected to be quite complicated and counterintuitive, if extrinsic noise leads to noise-induced ordering. It has been reported that noise may induce a bistable behaviour qualitatively different from what is possible deterministically [Samoilov *et al.* (2005)], induce stochastic focusing [Paulsson *et al.* (2000)], or increase the robustness of oscillations. Especially interesting would be to identify mechanisms through which noise-resistance appears due to the phase-repulsive property of the coupling. Taking into account the fact that stochastic effects in biomolecular systems have been recognized as a major factor, functionally and evolutionarily important, and that only a small amount of the recently discovered noise-induced phenomena in general dynamical systems have been identified in gene expression systems, this opens very wide perspectives for further research.

Another interesting question regards the influence of time delay on the phenomena discussed above. This issue has been discussed in single genetic oscillators [Chen and Aihara (2002)], where it has been seen that time delay generally increases the stability region of the oscillations, thereby making them more robust. In coupled oscillators, such as the ones discussed above, the effect of delay could be much more complicated. In particular, it was reported that delay in coupling may suppress synchronization without suppression of the individual oscillations [Rosenblum and Pikovsky (2004)]. Interestingly, delay in the coupling can seemingly change

the coupling from phase-attractive to phase-repulsive and *vice versa*. Since the multistability and multirhythmicity described here are the result of phase-repulsive interaction, time delay can probably induce such effects also in systems with phase-attractive coupling. Even more interesting would be to investigate the combined effect of delay, intrinsic noise, and cell-cell coupling. Recently it was shown that time delay in gene expression can induce oscillations even when system's deterministic counterpart exhibits no oscillations [Bratsun *et al.* (2005)].

An important aspect of synthetic biology is the design of smart biological devices or new intelligent drugs, through the development of *in vivo* digital circuits [Weiss *et al.* (2001)]. If living cells can be made to function as computers, one could envisage, for instance, the development of fully programmable microbial robots that are able to communicate with each other, with their environment and with human operators. These devices could then be used, e.g., for detection of hazardous substances or even to direct the growth of new tissue. In that direction, pioneering experimental studies have shown the feasibility of programmed pattern formation [Basu *et al.* (2005)], and the possibility of implementing logical gates and simple devices within cells [Hasty *et al.* (2002)]. We identify three perspective directions of this research. First is the construction of new biological devices capable to solve or compute certain problems [see e.g. Haynes *et al.* (2008)]. A second direction would be the identification of new dynamical regimes with extended functionality using standard genetic parts, as we have discussed here. Finally, it should be possible to add more levels of control, e.g. spatiotemporal control [Basu *et al.* (2004)] or temporal light-dependent control via encapsulation [Antipov and Sukhorukov (2004)] for precise regulation of synthetic genetic oscillators.

Finally it is worth noting that the investigation of synthetic genetic oscillators can profit greatly from techniques and methods transferred from other fields of science. Two areas are particularly relevant in this context: neural and electronic networks. Both neural and genetic networks make use of feedback and coupling mechanisms, and are significantly noisy [Swain and Longtin (2006)]. However, neural networks have attracted in recent years much more attention than genetic networks from scientists working in nonlinear dynamics. Neuroscientists have access to relatively long and clean time series of neural activity; such type of data are only now beginning to appear for genetic systems. This outlines a promising future to the combination of efforts in these two fields. On the other hand, direct analogies can be drawn between synthetic biology and established techniques in electrical engineering [Hasty *et al.* (2002)]. As a testbed of complicated experiments in the implementation of complex gene networks, electronic circuits provide much easier possibilities to investigate complex networks with similar topology and demonstrating complex dynamical phenomena [Buldú *et al.* (2005)].

Acknowledgments

E.U. acknowledges financial support from the Alexander von Humboldt Foundation. Financial support for E.U. and J.G.O. was provided by the European Commission (GABA project, contract FP6-2005-NEST-Path-043309). A.K. and J.K. acknowledge the GoFORSYS project funded by the Federal Ministry of Education and Research Grant Nr. 0313924 and the Network of Excellence BioSim (contract No. LSHB-CT-2004-005137), funded by the European Commission. A.Z. acknowledges financial support from Volkswagen-foundation, and E.V. from the Program Radiofizika (Russian Academy) and from RFBR Grant No. RFBR 08-02-00682. J.G.O. also acknowledges support from MEC (Spain, project FIS2006-11452 and I3 program).

References

Antipov, A. and Sukhorukov, G. (2004). Polyelectrolyte multilayer capsules as vehicles with tunable permeability, *Adv. Coll. Interface Sci.* **111**, pp. 49–61.

Atkinson, M. R., Savageau, M. A., Myers, J. T. and Ninfa, A. J. (2003). Development of genetic circuitry exhibiting toggle switch or oscillatory behavior in *escherichia coli*, *Cell* **113**, pp. 597–607.

Bar-Eli, K. (1985). On the stability of coupled chemical oscillators, *Physica D* **14**, pp. 242–252.

Basu, S., Gerchman, Y., Collins, C., Arnold, F. and Weiss, R. (2005). A synthetic multicellular system for programmed pattern formation, *Nature* **434**, pp. 1130–1134.

Basu, S., Mehreja, R., Thiberge, S., Chen, M. and Weiss, R. (2004). Spatiotemporal control of gene expression with pulse-generating networks, *Proc. Natl. Acad. Sci. U.S.A.* **101**, pp. 6355–6360.

Bratsun, D., Volfson, D., Tsimring, L. and Hasty, J. (2005). Delay-induced stochastic oscillations in gene regulations, *Proc. Natl. Acad. Sci. U.S.A.* **102**, pp. 14593–14598.

Buldú, J., García-Ojalvo, J., Wagemakers, A. and Sanjuán, M. (2005). Electronic design of synthetic genetic networks, *Int. J. Bif. Chaos* **17**, pp. 3507–3511.

Chen, L. and Aihara, K. (2002). A model of periodic oscillations for genetic regulatory systems, *IEEE Trans. Circ. Syst.* **49**, pp. 1429–1436.

Crowley, M. F. and Epstein, I. R. (1989). Experimental and theoretical studies of a coupled chemical oscillator: phase death, multistability and in-phase and out-of-phase entrainment, *J. Phys. Chem.* **93**, 6, pp. 2496–2502.

Dockery, J. D. and Keener, J. P. (2001). A mathematical model for quorum sensing in pseudomonas aeruginosa, *Bull. Math. Biol.* **63**, pp. 95–116.

Dolnik, M. and Marek, M. (1988). Extinction of oscillations in forced and coupled reaction cells, *J. Phys. Chem.* **92**, 9, pp. 2452–2455.

Elowitz, M. and Leibler, S. (2000). A synthetic oscillatory network of transcriptional regulators, *Nature* **403**, pp. 335–338.

Elowitz, M., Levine, A., Siggia, E. and Swain, P. (2002). Stochastic gene expression in a single cell, *Science* **297**, pp. 1183–1186.

Enright, J. (1980). Temporal precision in circadian systems: a reliable neuronal clock from unreliable components? *Science* **209**, 4464, pp. 1542–1545.

Ermentrout, B. (2002). *Simulating, analyzing and animating dynamical systems: a guide to XPPAUT for researchers and Students* (SIAM).

Fung, E., Wong, W. W., Suen, J. K., Bulter, T., Lee, S.-G. and Liao, J. C. (2005). A synthetic gene-metabolic oscillator, *Nature* **435**, pp. 118–122.

Fuqua, C. and Greenberg, P. (2002). Listening in on bacteria: acyl-homoserine lactone signaling, *Nat. Rev. Mol. Cell Biol.* **3**, pp. 685–695.

García-Ojalvo, J., Elowitz, M. B. and Strogatz, S. H. (2004). Modeling a synthetic multicellular clock: Repressilators coupled by quorum sensing, *Proc. Natl. Acad. Sci. U.S.A.* **101**, 30, pp. 10955–10960.

Gardner, T. S., Cantor, C. R. and Collins, J. J. (2000). Construction of a genetic toggle switch in *escherichia coli*, *Nature* **403**, pp. 339–342.

Gillespie, D. (1977). Exact stochastic simulation of coupled chemical reactions, *J. Phys. Chem.* **81**, pp. 2340–2361.

Gillespie, D. (2000). The chemical langevin equation, *J. Chem. Phys.* **113**, pp. 297–306.

Golomb, D., Hansel, D., Shraiman, B. and Sompolinsky, H. (1992). Clustering in globally coupled phase oscillators, *Phys. Rev. A* **45**, 6, pp. 3516–3530.

Hasty, J., McMillen, D. and Collins, J. J. (2002). Engineered gene circuits, *Nature* **420**, pp. 224–230.

Haynes, K., Broderick, M., Brown, A., Butner, T., Dickson, J., Harden, W. L., Heard, L., Jessen, E., Malloy, K., Ogden, B., Rosemond, S., Simpson, S., Zwack, E., Campbell, A. M., Eckdahl, T., Heyer, L. and Poet, J. (2008). Engineering bacteria to solve the burnt pancake problem, *J. Biol. Eng.* **2**, 1.

Herrero, R., Figueras, M., Rius, J., Pi, F. and Orriols, G. (2000). Experimental observation of the amplitude death effect in two coupled nonlinear oscillators, *Phys. Rev. Lett* **84**, 23, pp. 5312–5315.

Herzog, E. D., Aton, S. J., Numano, R., Sakaki, Y. and Tei, H. (2004). Temporal precision in the mammalian circadian system: A reliable clock from less reliable neurons, *J. Biol. Rhythms* **19**, pp. 35–46.

Herzog, E. D., Takahashi, J. S. and Block, G. D. (1998). Clock controls circadian period in isolated suprachiasmatic nucleus neurons, *Nature Neurosci.* **1**, pp. 708–713.

Honma, S., Shirakawa, T., Katsuno, Y., Namihira, M. and ichi Honma, K. (1998). Circadian periods of single suprachiasmatic neurons in rats, *Neurosci. Lett.* **250**, pp. 157–160.

Kaneko, K. and Yomo, T. (1994). Cell division, differentiation and dynamic clustering, *Physica D* **75**, pp. 89–102.

Kiss, I. Z. and Hudson, J. L. (2003). Chaotic cluster itinerancy and hierarchical cluster trees in electrochemical experiments, *Chaos* **13**, pp. 999–1008.

Klevecz, R. R. (1976). Quantized generation time in mammalian cells as an expression of the cellular clock, *Proc. Natl. Acad. Sci. USA* **73**, pp. 4012–4016.

Kobayashi, H., Kaern, M., Araki, M., Chung, K., Gardner, T. S., Cantor, C. R. and Collins, J. J. (2004). Programmable cells: Interfacing natural and engineered gene networks, *Poc. Natl. Acad. Sci. U.S.A.* **101**, pp. 8414–8419.

Koseska, A., Volkov, E., Zaikin, A. and Kurths, J. (2007a). Inherent multistability in arrays of autoinducer coupled genetic oscillators, *Phys. Rev. E* **75**, 3, p. 031916(8).

Koseska, A., Zaikin, A., García-Ojalvo, J. and Kurths, J. (2007b). Stochastic suppression of gene expression oscillators under intercell coupling, *Phys. Rev. E* **75**, p. 031917.

Kuznetsov, A., Kærn, M. and Kopell, N. (2004). Synchrony in a population of hysteresis-based genetic oscillators, *SIAM J. Appl. Math.* **65**, 2, pp. 392–425.

Liu, C., Weaver, D. R., Strogatz, S. H. and Reppert, S. M. (1997). Cellular construction of a circadian clock: Period determination in the suprachiasmatic nuclei, *Cell* **91**, pp. 855–860.

Lloyd, D. and Volkov, E. I. (1990). Quantized cell cycle times: interaction between a relaxation oscillator and ultradian clock pulses, *BioSystems* **23**, pp. 305–310.

Longtin, A. (1995). Mechanisms of stochastic phase-locking, *Chaos* **5**, pp. 209–215.

McMillen, D., Kopell, N., Hasty, J. and Collins, J. J. (2002). Synchronizing genetic relaxation oscillators by intercell signaling, *Proc. Natl. Acad. Sci. U.S.A.* **99**, 2, pp. 679–684.

Miller, M. B. and Bassler, B. L. (2001). Quorum sensing in bacteria, *Annu. Rev. Microbiol.* **55**, pp. 165–199.

Miyakawa, K. and Yamada, K. (2001). Synchronization and clustering in globally coupled salt-water oscillators, *Physica D* **151**, pp. 217–227.

Nakamura, W., Honma, S., Shirakawa, T. and ichi Honma, K. (2001). Regional pacemakers composed of multiple oscillator neurons in the rat suprachiasmatic nucleus, *Eur. J. Neurosci.* **14**, pp. 666–674.

Needleman, D. J., Tiesinga, P. H. E. and Sejnowski, T. J. (2001). Collective enhancement of precision in networks of coupled oscillators, *Physica D* **155**, pp. 324–336.

Okuda, K. (1993). Variety and generality of clustering in globally coupled oscillators, *Physica D* **63**, pp. 424–436.

Osipov, G. V., Kurths, J. and Zhou, C. (2007). *Synchronization in Oscillatory Networks*, Springer Series in Synergetics (Springer, Berlin, Germany).

Ozbudak, E., Thattai, M., Kurtser, I., Grossman, A. and van Oudenaarden, A. (2002). Regulation of noise in the expression of a single gene, *Nature Genet.* **31**, pp. 69–73.

Paulsson, J., Berg, O. and Ehrenberg, M. (2000). Stochastic focusing: fluctuation-enhanced sensitivity of intracellular regulation, *Proc. Natl. Acad. Sci. U.S.A.* **97**, 13, pp. 7148–7153.

Pikovsky, A. S. and Kurths, J. (1997). Coherence resonance in a noise-driven excitable system, *Phys. Rev. Lett.* **78**, pp. 775–778.

Riedel-Kruse, I. H., Muller, C. and Oates, A. C. (2007). Synchrony dynamics during initiation, failure, and rescue of the segmentation clock, *Science* **317**, 5846, pp. 1911–1915.

Rosenblum, M. and Pikovsky, A. (2004). Controlling synchronization in an ensemble of globally coupled oscillators, *Phys. Rev. Lett.* **92**, p. 114102.

Rosenfeld, N., Young, J. W., Alon, U., Swain, P. S. and Elowitz, M. B. (2005). Gene regulation at the single-cell level, *Science* **307**, pp. 1962–1965.

Samoilov, M., Plyasunov, S. and Arkin, A. (2005). Stochastic amplification and signalling in enzymatic futile cycles through noise-induced bistability with oscillations, *Proc. Natl. Acad. Sci. U.S.A.* **102**, pp. 2310–2315.

Somers, D. and Kopell, N. (1995). Waves and synchrony in networks of oscillators of relaxation and non-relaxation type, *Physica D* **89**, pp. 169–183.

Sprinzak, D. and Elowitz, M. B. (2005). Reconstruction of genetic circuits, *Nature* **438**, pp. 443–448.

Süel, G. M., Kulkarni, R. P., Dworkin, J., García-Ojalvo, J. and Elowitz, M. B. (2007). Tunability and noise dependence in differentiation dynamics, *Science* **315**, 5819, pp. 1716–1719.

Sveiczer, A., Novak, B. and Mitchison, J. M. (1996). The size control of fission yeast revisited. *J. Cell Sci.* **109**, pp. 2947–2957.

Swain, P., Elowitz, M. and Siggia, E. (2002). Intrinsic and extrinsic contributions to stochasticity in gene expressions, *Proc. Natl. Acad. Sci. U.S.A.* **99**, pp. 12795–12800.

Swain, P. and Longtin, A. (2006). Noise in genetic and neural networks, *Chaos* **16**, p. 026101.

Tsaneva-Atanasova, K., Zimliki, C. L., Bertram, R. and Sherman, A. (2006). Diffusion of calcium and metabolites in pancreatic islets: Killing oscillations with a pitchfork, *Biophys J.* **90**, pp. 3434—3446.

Tyson, J. and Kauffman, S. (1975). Control of mitosis by a continuous biochemical oscillation: Synchronization; spatially inhomogeneous oscillations, *J. Math. Biol.* **1**, pp. 289–310.

Ullner, E., Koseska, A., Kurths, J., Volkov, E., Kantz, H. and García-Ojalvo, J. (2008). Multistability of synthetic genetic networks with repressive cell-to-cell communication, Accepted to be published in Phys. Rev. E.

Ullner, E., Zaikin, A., Volkov, E. I. and García-Ojalvo, J. (2007). Multistability and clustering in a population of cellular genetic oscillators via phase repulsive cell-to-cell communication, *Phys. Rev. Lett.* **99**, p. 148103.

Volkov, E. and Stolyarov, M. (1991). Periodic attractors in two coupled relaxation oscillators, *Phys. Lett. A* **59**, pp. 61–66.

Volkov, E. and Stolyarov, M. (1994). Temporal variability in a system of coupled mitotic timers, *Biol. Cybern.* **71**, pp. 451–459.

Volkov, E. I. and Romanov, V. A. (1995). Bifurcations in the system of two identical diffusively coupled brusselators, *Physica Scripta* **51**, pp. 19–28.

Wang, W., Kiss, I. Z. and Hudson, J. L. (2000). Experiments on arrays of globally coupled chaotic electrochemical oscillators: Synchronization and clustering, *Chaos* **10**, pp. 248–256.

Wang, W., Kiss, I. Z. and Hudson, J. L. (2001). Clustering of arrays of chaotic chemical oscillators by feedback and forcing, *Phys. Rev. Lett.* **86**, pp. 4954–4957.

Weiss, R., Homsy, G. and Knight Jr., T. (2001). Toward *in vivo* digital circuits, in L. Landweber and E. Winfree (eds.), *Evolution as Computation (DIMACS Workshop)* (Springer-Verlag), pp. 275–295.

You, L., Cox III, R. S., Weiss, R. and Arnold, F. H. (2004). Programmed population control by cell-cell communication and regulated killing, *Nature* **428**, pp. 868–871.